CCF Transactions on Pervasive Computing and Interaction (2022) 4:88–102
https://doi.org/10.1007/s42486-021-00077-z

SURVEY PAPER

WiFi CSI-based device-free sensing: from Fresnel zone model to CSI-ratio model

Dan Wu[1] · **Youwei Zeng**[1] · **Fusang Zhang**[2] · **Daqing Zhang**[1,3]

Received: 1 June 2021 / Accepted: 8 September 2021 / Published online: 28 September 2021

Abstract
Over the past decade, WiFi CSI-based device-free sensing technology has shown great potential in smart homes, assisted living, and many other applications. While model-based device-free sensing approaches analyze and recognize human behaviors by constructing mathematical relationships among WiFi devices, environment, human position/posture, and received channel state information, they have attracted great attention because of the interpretable physical meaning and the ability to guide the WiFi-based sensing system design. In this paper, we retrospect two general-purpose sensing models, i.e., the Fresnel zone model and CSI-ratio model, and demonstrate how these two models are leveraged to extract insightful properties and support a variety of device-free sensing applications.

Keywords WiFi · Channel State Information (CSI) · Fresnel zone · Channel quotient · CSI ratio

1 Introduction

WiFi CSI-based sensing technology senses and recognizes human activity by leveraging the time-varying physical layer channel state information (CSI) extracted from commodity WiFi devices. WiFi sensing technology can be device-based or device-free, depending on whether a user needs to carry a WiFi device or not. Compared with the device-based solutions that users need to carry wireless devices, WiFi device-free sensing solutions do not need users' cooperation, making it possible and ideal for users to be monitored in naturally living environments, which have attracted wide research attention from both academia and industry in the past decade.

The history of WiFi-based device-free research begins from Youssef's pioneering work in 2007 (Youssef et al. 2007). They observed human motions can cause Received Signal Strength Indicator (RSSI) variations, so that human motion can be sensed passively in a device-free manner. Early studies have shown that by exploring RSSI variations or RSSI fingerprints, simple tasks such as human presence detection (Woyach et al. 2006; Youssef et al. 2007), indoor positioning (Bahl and Padmanabhan 2000), and respiration sensing (Abdelnasser et al. 2015) are possible. However, RSSI measurement is one-valued information which is rather coarse, it is not able to support complex sensing tasks. In contrast, WiFi devices began to report complex-valued CSI on OFDM sub-carrier granularity. Due to the rich physical-layer amplitude and phase information in multiple frequencies, the capability of sensing and understanding complex tasks is greatly enlarged. With the availability of CSI in many commodity WiFi cards since 2010, CSI-based WiFi sensing has made remarkable progress from enhancing existing RSSI-originated sensing tasks (Abdel-Nasser et al. 2013; Xiao et al. 2013; Vasisht et al. 2016; Wang et al. 2016; Zeng et al. 2019), to enabling a new set of human sensing applications, including gesture recognition (Abdelnasser et al. 2015; Tan and Yang 2016; Virmani and Shahzad 2017; Li et al. 2020), human identification (Wang et al. 2016; Zhang et al. 2016; Zeng et al. 2016; Zou et al. 2018), fall detection (Wang et al. 2016; Palipana et al. 2018), motion tracking (Li et al. 2017; Qian et al. 2018; Tan et al. 2019), activity recognition (Wang et al. 2014, 2015; Chen et al. 2018), as well as

✉ Daqing Zhang
dqzhang@sei.pku.edu.cn

Dan Wu
dan@pku.edu.cn

[1] Department of Computer Science and Technology, Peking University, Beijing, China

[2] Institute of Software, Chinese Academy of Sciences, Beijing, China

[3] Telecom SudParis, Institut Polytechnique de Paris, Paris, France

environmental sensing such as material sensing (Zhang et al. 2019) and soil sensing (Ding and Chandra 2019).

WiFi CSI-based device-free human sensing can be classified into two categories: pattern-based and model-based approaches (Wu et al. 2017). Pattern-based approaches, also known as data-driven machine learning approaches, recognize predefined sets of human behaviors by constructing mappings between human activities and CSI variation patterns (Wang et al. 2016; Wu et al. 2015; Li et al. 2017; Xin et al. 2018; Zhang et al. 2019; Wang et al. 2015; Zeng et al. 2016; Zou et al. 2018). They follow a common processing pipeline of data collection, signal processing, feature engineering, model training, and classification (Ma et al. 2019). Pattern-based approaches have the advantages of straightforward concept, simple algorithm design, and easy implementation. The implicit assumption of pattern-based approaches is that there is a one-to-one mapping between human activities and CSI patterns, and both the training data and test data follow the same distribution. However, this assumption is not necessarily true in wireless sensing because factors such as device location, human location, orientation, and room layout would all affect the mapping between human behavior and CSI patterns. Specifically, the same human behavior would produce very different CSI patterns, and different human behaviors might generate similar CSI patterns, thus breaking the one-to-one mapping between human behaviors and CSI patterns (Wu et al. 2017). As for the training data and testing data, since they are collected in different time and environment, it is not guaranteed that they follow similar distribution, because significant changes in the environment such as furniture position rearrangement, might make the received CSI follow a different distribution for the same human behavior. In addition, pattern-based approaches are also susceptible to the influence of feature selection. As a result, pattern-based approaches are not able to maintain stable sensing performance in real environment, even if a large amount of training data are collected in multiple settings.

As a comparison, model-based approaches attempt to quantitatively model the mathematical relationship between human locations, activities, environment and CSI, focusing on how changes in human position and activity lead to quantitative changes in CSI signal characteristics. Some of these model-based approaches extract signal parameters from CSI for sensing, such as angle of arrival (AoA) (Gjengset et al. 2014; Li et al. 2016), angle of departure (AoD) (Xie et al. 2019), time of flight (ToF) (Kotaru et al. 2015; Xie et al. 2019), and Doppler frequency shift (DFS) (Qian et al. 2017; Li et al. 2017). By combining these signal parameters, a sensing target can be located and tracked (Li et al. 2017; Qian et al. 2018; Xie et al. 2019; Wang et al. 2016; Tan et al. 2019; Wu et al. 2020). Other model-based approaches establish the association between human locations/behaviors and information such as CSI power frequency distribution, DFS, and Rayleigh distribution parameter, so it can be used for activity recognition (Wang et al. 2015) and room-level positioning (Li et al. 2020).

Unlike the mapping between CSI patterns and activities established by pattern-based approaches, the quantitative relationships constructed by model-based approaches have clear physical meaning. Therefore, using the model-based approaches it is possible to understand the impact of each signal parameter and the change of environment on the performance of the behavior sensing system, in order to design a robust sensing application. Despite the huge advantages of model-based approaches, the number of quantitative sensing models and their applications is quite limited, there are few general-purpose sensing models in the wireless sensing field. For example, the existing sensing models include AoA (Gjengset et al. 2014; Li et al. 2016), ToF (Kotaru et al. 2015; Xie et al. 2019), DFS (Qian et al. 2017; Li et al. 2017), and CSI-speed model (Wang et al. 2015). Out of these models, AoA, ToF, and DFS are only used for tracking and positioning, facing a lot of difficulties in extending to a wide range of sensing applications. Thus, it is hoped that general-purpose sensing models are proposed to guide the wireless sensing system design and support more sensing applications.

Fresnel zone model (Wu et al. 2016; Wang et al. 2016; Zhang et al. 2017) is a new general-purpose sensing model identified in the field of wireless sensing. Different from AoA, ToF, or DFS models that characterize only one parameter of the sensing target, Fresnel zone model establishes the geometrical relationship among WiFi transceiver position, sensing target position/direction, environment and the received CSI. It further reveals that the fluctuation patterns and frequency distribution of CSI are closely related to how the sensing target passes through the Fresnel zones in space. Because the Fresnel zone model depicts the relationship among diverse parameters of the device, human, and environment, it is possible to leverage this general-purpose model to extract diverse properties related to these parameters, explore the impact of individual and combined parameters on the sensing performance, and support a wide variety of sensing applications, such as respiration monitoring (Wang et al. 2016; Zeng et al. 2018), finger tracking (Wu et al. 2020), walking direction sensing (Wu et al. 2016) and trajectory tracking (Wang et al. 2017). What's more, Fresnel zone model helps us to understand why the same human activities would lead to diverse CSI variation patterns when sensing parameters such as a person's position and orientation are different, and different human activities might lead to similar CSI patterns (Zhang et al. 2021). It could even help to estimate the sensing limit of WiFi-based sensing systems.

The CSI-ratio model is another general-purpose one, which intends to reduce the amplitude noise and eliminate the phase offset in WiFi CSI-based sensing systems. As the CSI amplitude and phase of commodity WiFi devices is different from the ideal wireless channel, due to the fact that the amplitude contains the hardware noises generated in WiFi transceivers, and the phase contains random offset due to unsynchronized clock of WiFi transceivers. This problem prevents the extraction of ideal wireless channel from the received signal, leading to reduced sensing accuracy, short sensing distance, and incapability of supporting fine-grained sensing applications. Different from the amplitude denoising and phase compensation methods proposed in previous research, the CSI-ratio model effectively eliminates the amplitude noise and phase offset by constructing the CSI quotient of two antennas on a WiFi receiver, generating a new orthogonal base signal of amplitude and phase with high signal-to-noise-ratio. We have further proved that the properties of CSI-ratio model are very similar to those of the Fresnel zone model, thus maintaining a similar quantitative relationship between human behavior and CSI ratio. With the CSI-ratio model, a great number of sensing applications have been significantly improved, including the removal of detection blind spots (Zeng et al. 2018, 2019) and the extension of sensing range (Zeng et al. 2019) in human respiration sensing, while other new applications have also been enabled, such as multi-person respiration monitoring (Zeng et al. 2020) and centimeter-level finger motion tracking (Wu et al. 2020).

In this paper, we first introduce the two general-purpose sensing models, i.e., the Fresnel zone model and the CSI-ratio model, and show how to derive useful properties from these two models and how to utilize these properties to support a variety of sensing applications. By applying these models in different applications, we show that the model-based approaches are crucial in understanding and guiding the device-free wireless sensing system design. Leveraging the insights gained from general-purpose sensing models, we could effectively incorporate the data-driven approaches and exploit the full potential of wireless sensing systems in different application fields.

2 Fresnel zone model

The Fresnel zone concept originated from Augustin Fresnel's research on light's interference and diffraction in the early 19th century. When applied in the radio-based communication and sensing field, Fresnel zones refer to the series of confocal ellipsoids with two foci corresponding to the transmitter and receiver antennas. The geometry of Fresnel zones is defined by the wavelength of electromagnetic wave and the distance between two transceivers. For a given radio wavelength λ, considering Tx and Rx are two radio transceivers (see Fig. 1), Fresnel zones containing n confocal ellipsoids can be constructed by ensuring that

$$|T_xQ_n| + |Q_nR_x| - |T_xR_x| = n\lambda/2 \tag{1}$$

where Q_n is a point on the n_{th} ellipsoid. The innermost ellipsoid is defined as the first Fresnel zone (FFZ), the elliptical annuli between the first and second ellipsoids is defined as the 2nd Fresnel zone, and so on.

A sensing target in the Fresnel zones can reflect or diffract wireless signals, depending on its position. Diffraction dominates when the sensing target is within the FFZ, as the sensing target would block some of the signal propagation paths and only allows signal to propagate around it, causing remarkable drop in the received signal strength (Zhang et al. 2018). Conversely, reflection dominates when the sensing target is outside the FFZ, since most of RF signal energy is transmitted from the transmitter to the receiver via FFZ, and the reflected signal power off the sensing target is generally larger than that blocked by the sensing target, making reflection phenomina more significant than that of diffraction (Hristov 2000).

2.1 Diffraction model

The Fresnel zone diffraction model describes the relationship among the received signal, the distance between two transceivers and the physical parameters of a sensing target inside the FFZ (Zhang et al. 2018).

Assume a point P inside the FFZ, the distance from P to the line-of-sight (LoS) path formed by the transceiver pair is h, as shown in Fig. 1. M is the intersection point of the vertical line and LoS path. The path T_xR_x is then divided into two segments: $d_1 = |T_xM|$ and $d_2 = |MR_x|$. The path

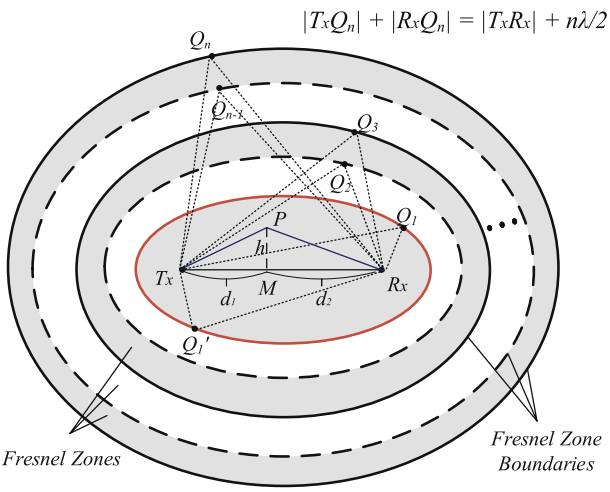

Fig. 1 The conceptual illustration of Fresnel zones

difference Δd between the path T_xPR_x and the LoS path T_xR_x is calculated by:

$$\begin{aligned}\Delta d &= |T_xP| + |PR_x| - |T_xR_x| \\ &= \sqrt{d_1^2 + h^2} + \sqrt{d_2^2 + h^2} - (d_1 + d_2) \\ &= d_1\sqrt{1 + \left(\frac{h}{d_1}\right)^2} + d_2\sqrt{1 + \left(\frac{h}{d_2}\right)^2} - (d_1 + d_2).\end{aligned} \tag{2}$$

When the target P is located inside the FFZ, we have $h \ll d_1$ and $h \ll d_2$. Therefore $(h/d_1)^2 \ll 1$ and $(h/d_2)^2 \ll 1$. By applying the approximation $\sqrt{1+x} \approx 1 + x/2$ when $x \ll 1$, Eq. 2 can be simplified as:

$$\Delta d \approx \frac{h^2}{2}\frac{(d_1 + d_2)}{d_1 d_2}. \tag{3}$$

The corresponding phase difference φ induced by this path length difference Δd can then be expressed as:

$$\varphi = \frac{2\pi\Delta d}{\lambda} = \pi h^2 \frac{(d_1 + d_2)}{\lambda d_1 d_2}. \tag{4}$$

Now let's denote v_{front} as a Fresnel diffraction parameter, which can be calculated as follows:

$$v_{\text{front}} = h_{\text{front}}\sqrt{\frac{2(d_1 + d_2)}{\lambda d_1 d_2}} \tag{5}$$

where h_{front} is the distance from target' front side to the line-of-sight (LoS) path formed by the transceiver pair, as illustrated in Fig. 2. Thus, the signal amplitude at the receiver due to front side diffraction $F(v_{\text{front}})$ is the integral of diffraction from the front side of the target to infinity:

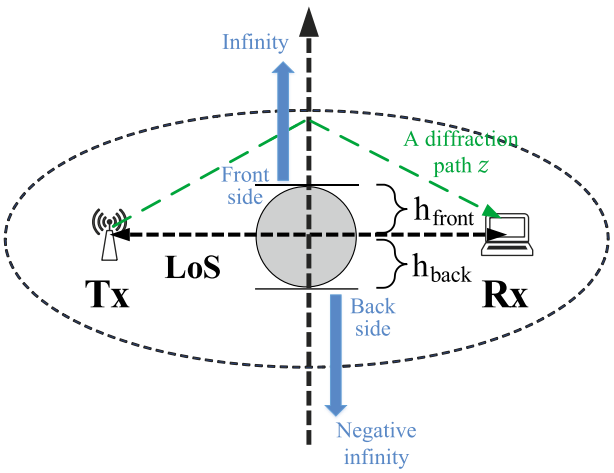

Fig. 2 The calculation of diffraction with an object inside the FFZ

$$F(v_{\text{front}}) = \frac{1+j}{2} \cdot \int_{v_{\text{front}}}^{\infty} \exp\left(\frac{-j\pi z^2}{2}\right) \mathrm{d}z, \tag{6}$$

where $\exp(-j\pi z^2/2)$ is the phase change for a specific diffraction path z. We accumulate all the signal paths diffracted from the front side of the target to infinity with respect to z from v_{front} to positive infinity. In the same way, we calculate the back side diffraction $F(v_{\text{back}})$ by integrating of all the paths diffracted from negative infinity to the back side of the target:

$$F(v_{\text{back}}) = \frac{1+j}{2} \cdot \int_{-\infty}^{v_{\text{back}}} \exp\left(\frac{-j\pi z^2}{2}\right) \mathrm{d}z. \tag{7}$$

Therefore, the total diffraction power is thus the sum of the signal paths from both sides:

$$Gain_{\text{Diff}} = 20\log\left|F(v_{\text{front}}) + F(v_{\text{back}})\right|. \tag{8}$$

The Fresnel zone diffraction model quantitatively describes the relationship between the received signal power and the target's position inside the inner Fresnel zones. Depending on the sensing target size and position, the received signal strength would change as the sensing target moves, as described by Eq. 8. No matter what the object shape is, the Fresnel zone diffraction model can always be used to guide human activity sensing in the inner Fresnel zones, such as for human respiration (Zhang et al. 2018) and activity recognition (Zhang et al. 2019).

2.2 Reflection model

The Fresnel zone reflection model describes the relationship among the received CSI signal, the distance between two transceivers, the location and orientation of the sensing target, and the environment while the sensing target is located outside the FFZ (Wu et al. 2016; Wang et al. 2016; Zhang et al. 2017).

For an RF signal of wavelength λ, as it travels a distance of d, its phase would change for $2\pi d/\lambda$. The received signal H is thus the superposition of the signals from all the paths, which can be denoted as

$$H = \sum A_k \exp(-i\frac{2\pi d_k}{\lambda}) \tag{9}$$

where k is the path number, d_k and A_k are the propagation length and power attenuation of the path k, respectively.

The Fresnel zone reflection model treats the received signal on a WiFi receiver as the superposition of two signal components, i.e., the static signal component H_s that does not change with time, containing LoS propagation and environmental reflection paths, and the dynamic signal component H_d that changes with time, containing human body reflection paths. In

case that the dynamic signal component mainly comes from a regular moving target, the changes of signals reflected from the sensing target are similar. Therefore, these dynamic signals can be regarded as coming from a single dynamic reflection path. The wireless channel $H(t)$ can then be denoted as the sum of the two phasor components on the complex plane (Wu et al. 2016; Wang et al. 2016):

$$H(t) = H_s + H_d = H_s + A(t)\exp(-i\frac{2\pi d(t)}{\lambda}) \tag{10}$$

where $A(t)$ is complex-valued attenuation coefficient of the dynamic reflection path.

We can further calculate the received signal power. Let the instant power of the LoS path d_0 be $|H_s|^2$ and that of the reflected path d_1 be $|H_d|^2$, let parameter $\theta(t)$ be the angle between the static phasor component H_s and dynamic phasor component H_d, the resulting instant CFR power $|H|^2$ at the receiver is given by the law of cosine (Wu et al. 2016; Zhang et al. 2017):

$$|H(t)|^2 = |H_s|^2 + |H_d|^2 + 2|H_s||H_d|\cos\theta(t) \tag{11}$$

apparently, Eqs. 10 and 11 describe the CSI signal in its complex-valued and power intensity forms, which exhibit circular-like and sinusoidal-like patterns, respectively.

As a sensing target moves outside the FFZ, the reflection path length $d(t)$ changes, and the dynamic phasor component rotates $\theta(t)$ accordingly. Once the sensing target crosses two consecutive Fresnel zones, which leads to one wavelength change for $d(t)$ and 2π change for $\theta(t)$, CSI exhibits a complete cycle change. The continuous motion of the sensing target in the Fresnel zones produces repeated patterns on both the CSI complex signal and CSI power intensity.

By deriving the dynamic reflection path $d(t)$ as a function of time t, we get the relative velocity of that path. The instant Doppler frequency shift $F(H(t))$ of CSI signal is defined as:

$$F(H(t)) = \frac{1}{2\pi}\frac{\mathrm{d}\theta(t)}{\mathrm{d}t} \tag{12}$$

$F(H(t))$ can be calculated by applying the short-time Fourier transform (STFT) on the time-domain CSI signal. The instant Doppler frequency shift (DFS) is numerically equivalent to the number of Fresnel zones crossed by a sensing target per second. For example, if the sensing target moves across two Fresnel zones in a second, then $\theta(t)$ rotates for 2π in that time, and instant DFS is 1Hz. The faster an object moves in a certain direction, the more Fresnel zones it passes through per second, and the greater the DFS is. The frequency distributions of CSI power $|H|^2$ follows similar patterns as DFS but has no sign information (Wang et al. 2015).

2.3 Location-dependency problem revealed by reflection model

An important finding and implication of the Fresnel zone reflection model is that it reveals the fact that the CSI signal varies with the sensing target's location and orientation change for the same human activity. That is to say, the same kind of human activities performed at different location and orientation often lead to different CSI patterns, while different activities performed at specific location and orientation may produce similar CSI patterns. We call it the "location-dependency problem" in device-free wireless sensing. We illustrate it using micro-scale and macro-scale activity sensing as examples. Micro-scale motions, such as breathing and finger motion, span less than one Fresnel zone, which corresponds to an incomplete cycle in the received CSI signal waveform. Macro-scale motions, such as human daily activity and walking, span multiple Fresnel zones, which causes a repeated multi-cycle pattern in the received CSI signal.

For macro-scale motions, the reflection model indicates that CSI signal patterns are determined by the way a sensing target passes through the Fresnel zones. We take a simple straight-line move as an example. As illustrated in Fig. 3, activities 1 and 2 are same in direction but different in motion distance, activities 3 and 4 are identical in length and direction but different in starting position; activities 2 and 3 are same in length and starting position but different in orientation. Depending on the number of Fresnel zone crossed, the motions in the above four cases produce different number of fluctuations in the received CSI waveform. Assuming constant moving speed in all the cases, we expect

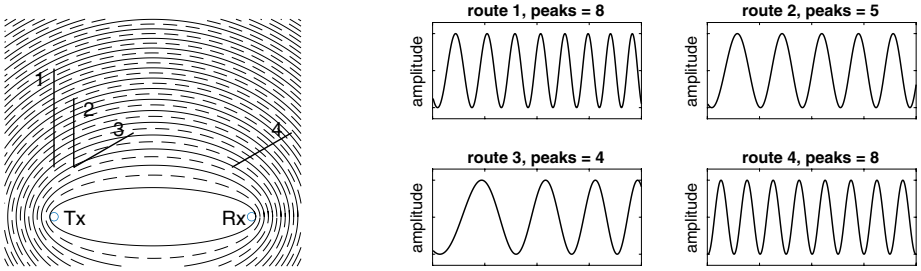

(a) The four cases of activities (b) The CSI signal

Fig. 3 The CSI signals are location, orientation, and activity magnitude dependent (from Zhang et al. (2021) ©Springer)

twice the CSI signal frequency in case 1 and 4 as of in case 3, since the subject crosses half the number of Fresnel zones in case 3 than other cases within the same time duration. If the activities are performed at different speed for each case, the frequency of the CSI signal varies accordingly. This simple example indicates the patterns of the received CSI for the same activity are location and orientation-dependent. Similarly, two movements with different positions and orientations may also produce identical signal pattern, as shown in case 1 and 4. In addition to position and orientation, the motion speed also affects CSI signals. Although there will be the same number of fluctuation for the same motion path, faster movement will produce higher CSI signal frequency.

For micro-scale motions, the reflection model indicates that the CSI signal is always a fragment of a complete cycle. The CSI pattern is not only affected by the moving direction and position of the sensing target, but also highly correlated with the initial in-zone position, i.e., the relative position related to the Fresnel zone boundaries (Wu et al. 2020). A centimeter difference in position will make a big difference in the received CSI. Figure 4 shows the received CSI patterns corresponding to drawings of the letter 'd' in the air with a finger in three cases. Case a and case b are different in drawing size, while case b and case c are different in their initial in-zone drawing positions. The three cases show totally different CSI patterns. For detailed analysis, please refer to Wu et al. (2020).

As a special case, for regular micro-scale motions such as breathing, the CSI signal cycle is mainly generated by the repetitive motion of the chest. In each cycle, the received signal is a fragment of a sinusoidal cycle (Wang et al. 2016). If the fragment lies fully in the monotonically changing part of the sinusoidal cycle, the CSI pattern of respiration is regular and thus is easy to detect. Otherwise, the CSI appears irregular and the respiration is unlikely to be extracted from the received CSI. Accordingly, within each Fresnel zone, the worst human location for respiration sensing is around the boundary, while the best location appears in the middle of the Fresnel zone. As a result, a series of interleaved blind detection spots could appear when sensing respiration with CSI amplitudes (Wang et al. 2016).

2.4 Sensing human with Fresnel zone model

Fresnel zone model is a general-purpose model. It is flexible in supporting a wide range of applications by exploiting different model properties.

2.4.1 Exploiting multiple subcarriers

The OFDM in WiFi systems divides the whole bandwidth into multiple subcarriers of different frequencies. Each of the subcarriers has its own Fresnel zones. The Fresnel zone of a subcarrier with a shorter wavelength is slightly smaller than that of a subcarrier with a larger wavelength. By considering all the subcarriers, the multi-frequency Fresnel zone model shows regular precedence patterns as a sensing target moves.

We have learned that the phase parameter θ determined the phase of sinusoidal waves in Eq. 11. For two subcarriers of wavelength λ_1 and λ_2, the phase difference $\Delta\theta$ between two subcarriers can be quantified as:

$$\Delta\theta = 2\pi(d_1 - d_0)(\frac{1}{\lambda_1} - \frac{1}{\lambda_2}) = \frac{2\pi\Delta d\Delta f}{c} \tag{13}$$

where d_1 and d_0 represent the length of the reflected path and the LoS path, respectively. Δf represents the frequency interval between the two subcarriers. It is worth mentioning that Eq. 13 describes a simple case that no static environmental reflection other than the LoS path exists. In a multi-path rich environment, the accurate phase delay is no more preserved, but the waveform precedence relationship of subcarriers preserves roughly.

WiDir (Wu et al. 2016) is a walking direction estimation system. It gives an example of how to leverage the precedence of multi-frequency Fresnel zones for rough direction sensing. As the shape size of elliptical Fresnel zones differs on subcarriers, if a person moves inward/outward the Fresnel zones, she/he would cross the Fresnel zone boundaries of different subcarriers in sequence and generate increasing/decreasing time delays between a fixed pair of subcarriers, as illustrated in Fig. 5. The inward/outward walking direction can be determined by inspecting the CSI time delay between subcarrier pairs.

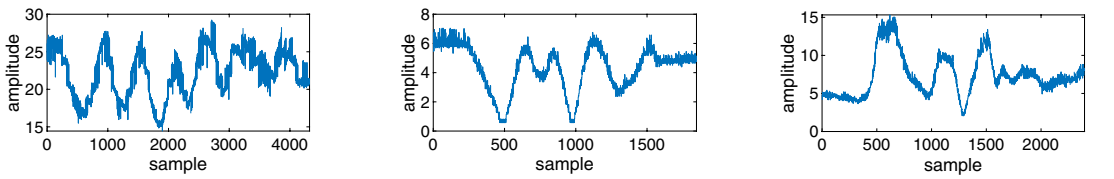

(a) drawing size: 4x6 cm @position 1 (b) drawing size: 3x4 cm @position 1 (c) drawing size: 3x4 cm @position 2

Fig. 4 the recorded CSI waveforms for the same drawing of letter 'd' of different drawing sizes and in-zone positions show different patterns

MFDL (Wang et al. 2017) is another example that exploits multi-frequency Fresnel zones for human positioning. It uses the fact that the length difference Δd between the reflection path d_1 and the LoS path d_0 is linearly proportional to the phase delay $\Delta\theta$ on subcarriers, as described in Eq. 13. MFDL develops an algorithm to extract the phase delay from CSI of multiple subcarriers, then it estimates the reflection path length d_1 based on it. MFDL achieves a median localization error of 45cm for a walking person in an outdoor environment.

2.4.2 Exploiting multiple antennas

In a modern WiFi device using MIMO technology, there are multiple antennas installed. Each combination of the transmitter and receiver antennas forms its Fresnel zones. The spatial discrepancy brings additional opportunities.

Researchers at Hong Kong Polytechnic University demonstrate a multi-person respiration sensing system with multi-antenna Fresnel zones (Yang et al. 2018). The blind detection areas of Fresnel zones are exploited to 'hide' people so that one's respiration at detectable area is easily detectable without interference. By placing WiFi transceiver antennas carefully, only the person in a certain location can affect the received CSI on a transceiver antenna pair. With the 2×2 antenna setting in commodity WiFi, they support respiration monitoring for up to three persons. The concept of multi-person respiration sensing with multiple antennas is illustrated in Fig. 6.

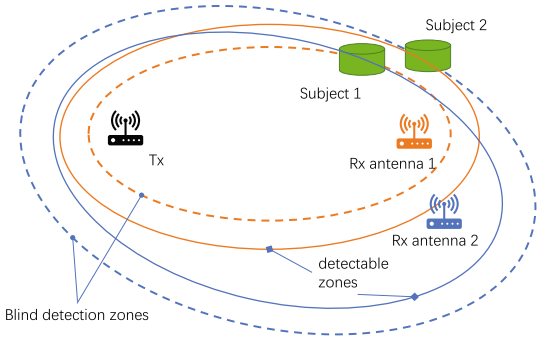

Fig. 6 Illustration of multi-person respiration with multi-antenna Fresnel zones. By placing antennas carefully, subject 1 is at the blind detection spots of antenna 1, so that only antenna 2 captures the respiration of subject 1. Similarly, the respiration of subject 2 can only be captured by antenna 1

2.4.3 Exploiting multiple links

A single transmitter-receiver link provides a particular viewing-angle for the motion of a sensing target, and it suffers from the location-dependency problem. Naturally, we can bring in more WiFi links of multiple viewing-angles to supply more sensing information.

A simple yet powerful placement of WiFi transceivers uses one transmitter and two receivers in a way that the two WiFi links are placed perpendicular to each other, as illustrated in Fig. 7a. In this setting, the motion or the activity performed by the sensing target can be observed from two orthogonal views. This setting is adopted by several applications that sense and track human motion in the 2D plane (Wu et al. 2016; Li et al. 2017; Wu et al. 2020), as the two sets of Fresnel zones constitute crossed grids that provide well-balanced information from two dimensions.

WiDir (Wu et al. 2016) uses this setting to estimate the accurate walking direction of a person in the 2D plane. As discussed in Sect. 2.4.1, WiDir gets the inward/outward moving information with multi-frequency Fresnel zones. The walking length in x or y axis across Fresnel zones is then approximated by counting the number of Fresnel zones crossed. Putting together the two pieces of information, a scalar displacement (with sign) comes out of each WiFi-link. By modeling the perpendicular WiFi links as x-axis and y-axis, WiDir successfully estimates the 2D walking direction of a person.

IndoTrack (Li et al. 2017) and FingerDraw (Wu et al. 2020) use the same 2-link setting for human tracking and finger motion tracking. They quantify the crossed Fresnel zones with a group of elliptic equations other than the

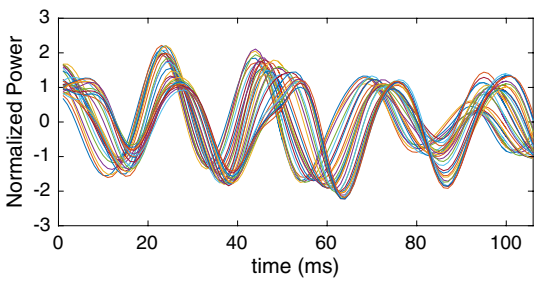

Fig. 5 The delayed waveform for all 30 subcarriers as a person walks (from Wu et al. (2016) ©ACM)

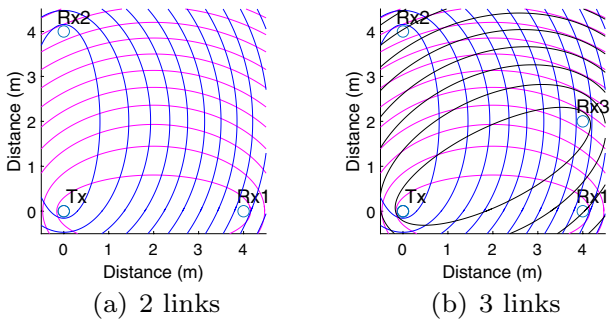

(a) 2 links (b) 3 links

Fig. 7 Illustration of crossed Fresnel zones formed by multiple WiFi links

oversimplified squared grids as did in WiDir to support more precise tracking and localization. Moreover, they improve the distance estimation accuracy. IndoTrack estimates the displacement on each device-link with DFS information based on the proposed DopplerMUSIC algorithm (Li et al. 2017), and FingerDraw extracts centimeter-level motion on each device-link with the help of the CSI-ratio model.

The setting of multi-link Fresnel zones also benefits activity recognition. Human activities often involve motions of multiple body parts. When observing from different viewing angles, the reflected WiFi signals come from different body surfaces which worsen the 'location-dependency' problem. By deploying multiple links such as the setting in Fig. 7b, we can capture CSI from more viewing-angles. Thus, we have more information and have a better chance to solve this problem. For instance, WiDar 3.0 (Zheng et al. 2019) gives a potential orientation-independent solution for gesture recognition using the setting of three WiFi links.

It is worth mentioning that when more WiFi links exist, we can combine the Fresnel zone reflection and diffraction models to better support human activity sensing in a home. While walking or performing activities, a person may cross the line-of-sight of a WiFi link, which is depicted by diffraction model. At the same time, she/he also leads to CSI variations on other links that are depicted by reflection model. With the abundant information obtained by these models, it is possible to infer human contexts and support the continuous sensing of daily activities.

3 CSI ratio model

The Fresnel zone model establishes a geometrical relationship among the ideal CSI signal, the relative distance between two WiFi transceivers, and the relative location and orientation of the sensing target with respect to the two WiFi transceivers. Unfortunately, as the WiFi transmitter and receiver are two separate devices each uses its own hardware clock, there is synchronization error between them. The error include the carrier frequency offset (CFO) and sampling frequency offset (SFO) (Kotaru et al. 2015; Xie et al. 2015), which randomly affects CSI phase and makes it unusable for human sensing in practice. As a consequence, lots of existing WiFi-based sensing approaches employ only the coarse CSI amplitude readings for sensing, leading to several critical limitations, as shown in Sect. 2.3. CSI-ratio model bridges the gap between the ideal CSI in Fresnel zone model and the real-life CSI retrieved from commodity WiFi.

3.1 Definition of CSI ratio

Observing the fact that the CSI readings retrieved from different antennas at the same receiver contain very similar hardware noise (Zeng et al. 2019; Wu et al. 2020; Zeng et al. 2020), we propose to use CSI ratio, which is defined as the quotient of CSI readings between two antennas (Zeng et al. 2019; Wu et al. 2020; Zeng et al. 2020), as a new base signal for sensing:

$$H_r(f,t) = \frac{H_1(f,t)}{H_2(f,t)} \tag{14}$$

where $H_1(f,t)$ is the complex-valued CSI of the first antenna and $H_2(f,t)$ is that of the second antenna.

3.2 Noise cancellation with CSI ratio

A prominent benefit of CSI ratio is that it cancels the amplitude noise and phase offset in commodity WiFi devices effectively. Since two antennas on the same receiver share the same RF chain and clock, the amplitude noise and the random phase offset in each antenna of the same receiver are almost identical. Therefore, the division operation cancels them. After that, we get the ratio of two ideal air channels, as described in Eq. 15:

$$\frac{H_1(f,t)}{H_2(f,t)} = \frac{\cancel{A(f,t)e^{-j2\pi\triangle\theta(f,t)}}H_{air1}(f,t)}{\cancel{A(f,t)e^{-j2\pi\triangle\theta(f,t)}}H_{air2}(f,t)} = \frac{H_{air1}(f,t)}{H_{air2}(f,t)} \tag{15}$$

where $A(f,\ t)$ is the scaling noise in CSI amplitude, $e^{-j2\pi\Delta\theta(f,t)}$ is the random offset in CSI phase, H_{air1} and H_{air2} are the ideal air channels between the transmitter antenna to the receiver antenna 1 and antenna 2, respectively.

To visualize the effect of noise cancellation with CSI ratio, we conduct a simple experiment with a setup similar to Fig. 3a. Based on the Fresnel zone model, five peaks/valleys are expected to appear on the recorded CSI amplitude waveform. Fig. 8a, b show the raw CSI amplitudes retrieved from two antennas at the same receiver. We can see in Fig. 8a that the plate movement-induced amplitude variation pattern is buried in the noise. The amplitude variation pattern in Fig. 8(b) is slightly clearer. As shown in Fig. 8d, e, the raw CSI phases of the two antennas jump randomly, making them unusable. In comparison with the real-world CSI from each individual antenna, Fig. 8c, f show the amplitude and phase of CSI ratio, respectively. We can clearly observe five peaks/valleys in both amplitude and phase waveforms. With the division operation, most of the noise in the original CSI amplitude and the time-varying phase offset are successfully canceled out, providing a new orthogonal base signal with a high SNR for human sensing.

3.3 CSI ratio model and Möbius transformation

Another attractive advantage of the CSI ratio is that the CSI ratio of two antennas retains the signal variation patterns

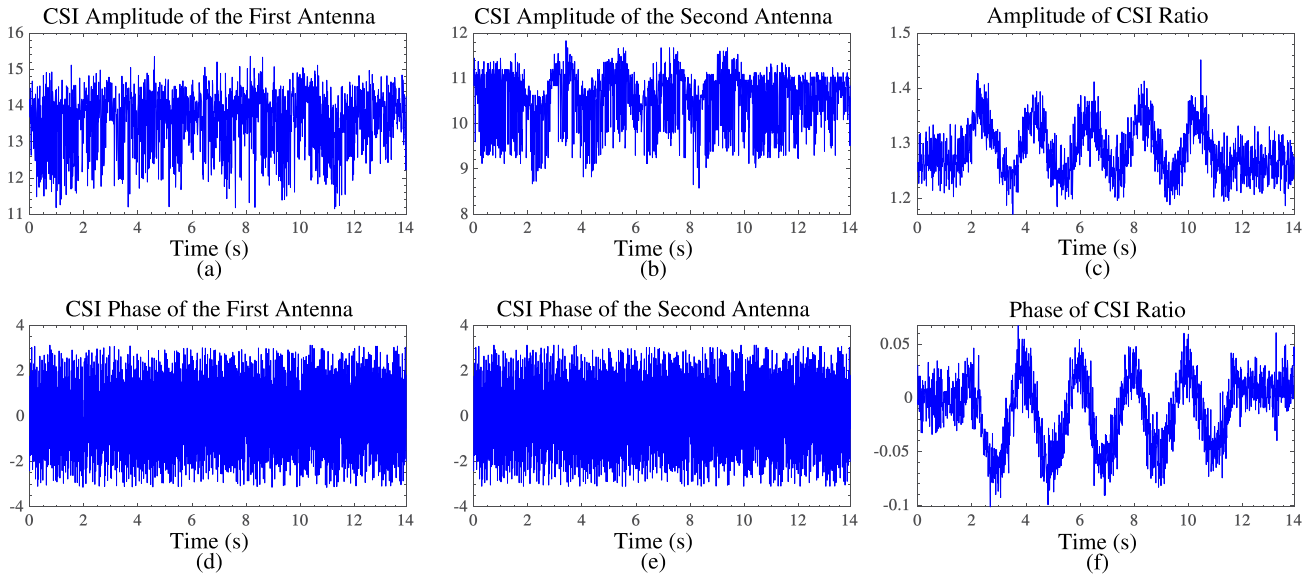

Fig. 8 Comparison of raw CSI and CSI ratio while sensing the plate movements (from Zeng et al. (2020) ©IEEE)

that can be used for sensing. Through mathematical transformation, it can be mapped to the movement of the sensing targets.

In the case that there is only one moving target, we can rewrite CSI ratio according to Eqs. 10 and 14 as:

$$\begin{aligned} H_r(f,t) &= \frac{H_{s,1} + A_1 e^{-j2\pi \frac{d_1(t)}{\lambda}}}{H_{s,2} + A_2 e^{-j2\pi \frac{d_2(t)}{\lambda}}} \\ &= \frac{A_1 e^{-j2\pi \frac{d_1(t)}{\lambda}} + H_{s,1}}{A_2 e^{-j2\pi \frac{d_2(t)-d_1(t)}{\lambda}} e^{-j2\pi \frac{d_1(t)}{\lambda}} + H_{s,2}} \\ &= \frac{\mathcal{A}\mathcal{Z} \Downarrow \mathcal{B}}{\mathcal{C}\mathcal{Z} \Downarrow \mathcal{D}} \end{aligned} \tag{16}$$

where $d_2(t) - d_1(t)$ is the difference in target-reflection path length between two close-by antennas that can be seen as a constant (Zeng et al. 2018), the coefficients $\mathcal{A}$, $\mathcal{B}$, $\mathcal{C}$, $\mathcal{D}$ are complex constants, and $\mathcal{Z} = e^{-j2\pi \frac{d_1(t)}{\lambda}}$ is a unit complex variable, whose phase represents the change in reflection path length. Mathematically, Eq. 16 is exactly in the form of Möbius transformation (also known as linear fractional transformation) (Schwerdtfeger 1979).

Learning from the properties of Möbius transformation, we know that if the reflection path length $d_1(t)$ changes one wavelength, the CSI ratio would rotate for a full circle on complex plane, and if it changes less than one wavelength, the CSI ratio just rotates for a circular arc. Besides, assuming the magnitude of static component $H_{s,2}$ is larger than that of dynamic component $A_2 e^{-j2\pi \frac{d_2(t)}{\lambda}}$, if the reflection path length $d_1(t)$ increases, the arc in CSI ratio rotates clockwise; otherwise, it rotates counterclockwise. Apparently, the properties of CSI ratio model are similar to those of Fresnel zone model. Benefiting from the high SNR and orthogonal nature of CSI ratio signal, we can precisely derive the reflection path length change from it, which would lay the foundations for fine-grained human sensing.

3.4 CSI ratio model variations

In the previous section, we discussed a simple case of CSI ratio of two antennas. When there are more antennas, CSI ratio can be applied to any two antennas, leading to many more combinations. Therefore, several model variants deserve in-depth study.

Assuming that we have P transmitting antennas and Q receiving antennas, as we are able to obtain one CSI reading from each antenna pair, there are PQ CSI readings in total at one timestamp for each sub-carrier. By selecting one CSI reading as the numerator of CSI ratio and another one as the denominator, we will get $A_{PQ}^2 = PQ(PQ-1)$ CSI ratios for human sensing.

First, if there is only one transmitting antenna and one receiving antenna, would the signal ratio method fail to work? In fact, we may be able to employ the CSI readings from multiple sub-carriers to construct CSI ratio. The key to achieve this goal is to find out the relationships between the CSI phase offsets from different sub-carriers.

Second, how can we fuse the data from different CSI ratios when multiple antennas or devices are provided? Actually, each of these CSI ratios can be viewed as an information source, providing us a unique "view" of the observed target. Intuitively, it allows us to combine the information

carried by the multiple views to improve the sensing accuracy. On the one hand, we could adjust the numerator of CSI ratio by a weighted sum of different CSI ratios to enhance the signals reflected off the target, which may help to further extend the sensing range and improve the sensing accuracy. On the other hand, we could adjust the weights of the sum to cancel out the unwanted reflection signal.

Third, in Eq. 16, we just consider one moving target, how about the scenario when multiple persons are present? It's interesting to investigate the properties of CSI ratio in these scenarios, and it may help to solve the challenging problem of multi-person sensing.

3.5 Sensing human with CSI-ratio model

CSI ratio can be used to accomplish many sensing tasks by exploiting its model properties.

3.5.1 Sensing micro-scale activities by exploiting orthogonality

CSI ratio is a complex number, whose amplitude and phase are orthogonal and complementary to each other. Leveraging this feature, we can not only better capture the subtle changes of the signal corresponding to the tiny motion (e.g., respiration monitoring Zeng et al. 2019), but also to extract a consistent signal pattern corresponding to the same gesture by combining the two information (e.g., gesture recognition Wu et al. 2020).

Respiration monitoring. Prior work (Zhang et al. 2017; Liu et al. 2014; Wang et al. 2016) takes the raw CSI amplitude from one antenna to track the millimeter-level chest movement caused by respiration. All of them faces the "blind spot" issues, that is, human respiration cannot be effectively detected at certain locations even when the target is close to the sensing devices. As a comparison, we take the CSI ratio as the base signal to extract respiration pattern by applying the PCA method (Zeng et al. 2019) that elaborately combining the orthogonal amplitude and phase of CSI ratio, as shown in Fig. 9. Our experiments show that, by exploiting the CSI ratio, the "blind spots" issue can be fully solved, enabling respiration monitoring with a higher accuracy.

Gesture recognition. As previously revealed, the mapping between target movement and CSI amplitude variation is location-dependent, resulting in unstable activity recognition accuracy. Fortunately, the division operation in obtaining CSI ratio cancels out the time-varying phase offset, thus enabling us to utilize the phase information that is unusable with one single antenna. We take the finger gesture recognition described in Fig. 4 as an example. We show how to utilize the complex-valued CSI ratio to extract a consistent feature that helps to improve the accuracy in recognizing different gestures. We choose the radian change of the arc that the CSI

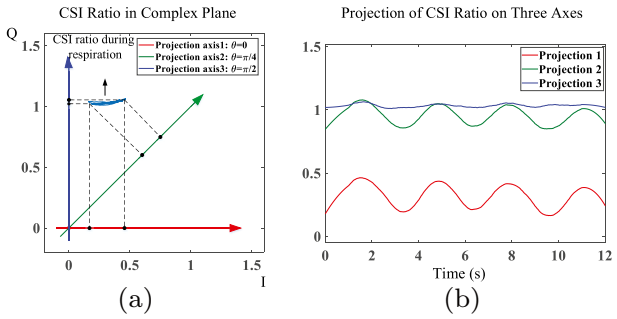

Fig. 9 Example of projecting a time series of two-dimensional CSI ratio during respiration in complex plane: **a** CSI ratio and three projection axes ($\theta = 0, \pi/4, \pi/2$); **b** projection results on three corresponding axes in (**a**). According to the PCA method, the projection of $\theta = 0$ is chosen as the respiration pattern (from Zeng et al. (2019) ©ACM)

ratio generates on complex plane as the feature. In this way, for the finger drawing in Fig. 4, the same gesture performed at different locations generates the same feature pattern in the three cases (Fig. 10). This is exactly what we want for gesture recognition.

3.5.2 Sensing motion by exploiting Fresnel zone model equivalency

CSI-ratio model has a strong resemblance to the Fresnel zone reflection model. The signals of both CSI and CSI ratio show similar circular-patterns on the complex plane as an object moves. Therefore, we can bypass the sanitizing to the phase offset on raw CSI, as did in most works (Kotaru et al. 2015; Xie et al. 2015, 2019), and focus on the CSI ratio instead. Taking advantage of this property, we have the fine-grained sub-wavelength motion sensing capability.

FingerDraw (Wu et al. 2020) is a centimeter-level finger motion tracking system. Compared with the typical WiFi wavelength in the 5GHz band (less than 6cm), the motion of finger strokes in the air can be shorter than a wavelength, which corresponds to a portion of a complete circular-pattern on the complex plane for the CSI ratio signal, i.e, a circular arc. As illustrated in Fig. 11, by measuring the phase change on the CSI ratio arc, the signal propagation length change that reflects off the finger is calculated. With the information from the crossed Fresnel zones of the two perpendicular placed WiFi links, FingerDraw approximates the 2D finger motion iteratively.

3.5.3 Sensing multiple persons by exploiting linear additive property

CSI ratio in the form of Möbius transformation models a single target. By exploiting linear additive property and extending Eq. 16, we can use the CSI ratio model to sense multiple

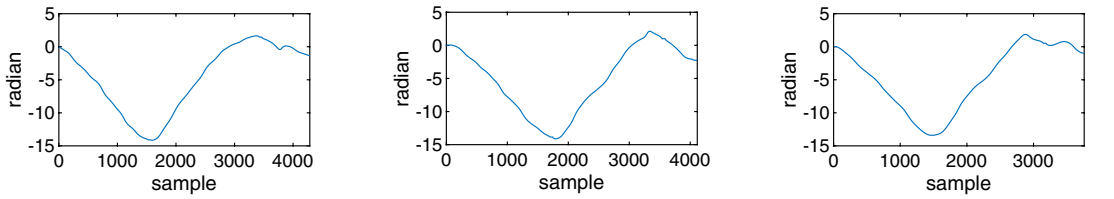

(a) drawing size: 4x6 cm @position 1 (b) drawing size: 3x4 cm @position 1 (c) drawing size: 3x4 cm @position 2

Fig. 10 The transformed phases of letter 'd' in three cases described in Fig. 4 now show consistent features

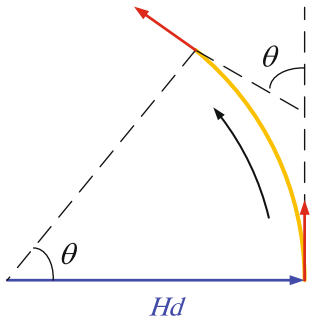

Fig. 11 The radian change of the arc can be measured easily as the tangent slope changes on that arc

targets. In this case, the numerator and denominator of CSI ratio are not necessary to be the CSI readings of one certain antenna, it is a weighted sum of several antennas' CSI readings:

$$\begin{aligned} & w_1 H_1(f,t) + w_2 H_2(f,t) \\ & = w_1(\mathcal{A}\mathcal{Z}\Downarrow\mathcal{B}) + w_2(\mathcal{C}\mathcal{Z}\Downarrow\mathcal{D}) \\ & = (w_1\mathcal{A} + w_2\mathcal{C})\mathcal{Z} + (w_1\mathcal{B} + w_2\mathcal{D}) \\ & = \mathcal{E}\mathcal{Z}\Downarrow\mathcal{F} \end{aligned} \tag{17}$$

where w_1 and w_2 are the weights of the sum of two CSI readings. By adjusting the weights, we may get some interesting observations. For example, we could cancel out the dynamic reflection signal if $\mathcal{E} = 0$.

We take multi-person respiration monitoring as an example to show how to utilize this variation of CSI ratio for sensing. In the presence of N breathing persons, the CSI readings of M antenna pairs can be denoted as follows:

$$\begin{cases} H_1(f,t) & = e^{-j\phi(t)}(\sum_{i=1}^{N} a_{1,i}\mathcal{Z}_i + b_1) \\ H_2(f,t) & = e^{-j\phi(t)}(\sum_{i=1}^{N} a_{2,i}\mathcal{Z}_i + b_2) \\ & ..... \\ H_M(f,t) & = e^{-j\phi(t)}(\sum_{i=1}^{N} a_{M,i}\mathcal{Z}_i + b_M) \end{cases} \tag{18}$$

where $H_1(f,t)$ is the first CSI reading, $H_M(f,t)$ is the M^{th} CSI reading, $\phi(t)$ is the time-varying phase offset, $\mathcal{Z}_i$ is the i^{th} person's respiration signal and b_i is the corresponding background static signal. We sum up the M CSI readings by a certain weight to cancel out the respiration signal $\mathcal{Z}_i$ (Zeng et al. 2020):

$$\begin{aligned} H_{ref}(f,t) &= \sum_{i=1}^{M} w_i H_i(f,t) \\ &= \sum_{j=1}^{N}(\sum_{i=1}^{M} w_i a_{i,j})\mathcal{Z}_j + \sum_{i=1}^{M} w_i b_i \end{aligned} \tag{19}$$

where w_i is the weight that satisfies $\sum_{i=1}^{M} w_i a_{i,j} = 0$ for $j = 1, 2, \ldots, N$. We call $H_{ref}(f,t) = \sum_{i=1}^{M} w_i b_i$ the reference CSI as it's not affected by the breathing persons. Then, the reference CSI $H_{ref}(f,t)$ is chosen as the denominator of CSI ratio while the original CSI $H_i(f,t)$ is the numerator of CSI ratio. The advantage of such a variation of CSI ratio is that, the time-varying phase offset is successfully canceled out while the linearity is kept so that we can use ICA (Independent Component Analysis) method to separate the respiration signal $\mathcal{Z}_i$ from the processed CSI (Sánchez 2002).

3.6 Applications using other wireless signals

The Fresnel zone model and CSI-Ratio model can be applied to other wireless technologies, including 4G LTE (Chen et al. 2020), LoRa (Zhang et al. 2020), RFID (Chen et al. 2019), etc. Although these wireless technologies use different signal modulations, they have the common characteristic of separated transmitter and receiver, and face similar issues such as CFO and SFO offsets as appeared in WiFi-based sensing. Therefore, it is possible to cancel the measurement noise and model the physical features of the sensing target with the CSI-Ratio model. We use LoRa sensing as an example to illustrate it.

According to the recent long range LoRa sensing work (Zhang et al. 2020), the signal ratio can also be used to eliminate the base chirp band and phase offsets. Note that LoRa signal for sensing can be denoted as:

$$Rx(t) = e^{j(\pi kt^2+\theta_c+\theta_s)}\left(H_s + a(t)e^{-j\frac{2\pi d(t)}{\lambda}}\right) \tag{20}$$

where $e^{j\pi kt^2}$ is the LoRa chirp based band signal, $\theta_c = 2\pi\Delta ft$ is the carrier frequency offset, while Δf is the frequency drift caused by unsynchronized clocks at the transmitter and receiver, which has a significant influence on signal phase. θ_s is the phase error introduced by sampling frequency offset. H_s is the environment static signal called static vector in the I/Q space. $a(t)e^{-j\frac{2\pi d(t)}{\lambda}}$ is the dynamic vector, which contains the signal reflected from the motion target. In order to use the LoRa signal for sensing, we need to remove the high frequency base-band chirp signal and the phase offsets, so that only the movement information of the target retains.

Thus, the signal division operation is performed on the LoRa gateway equipped with two antennas. This offers opportunity to remove the varying random frequency offset, which can be derived as follows:

$$SR(t) = \frac{R_1(t)}{R_2(t)} = \frac{\cancel{e^{\pi kt^2+\theta_c+\theta_s}}\left(H_{s1} + a_1(t)e^{-j\frac{2\pi d(t)}{\lambda}}\right)}{\cancel{e^{\pi kt^2+\theta_c+\theta_s}}\left(H_{s2} + a_2(t)e^{-j\frac{2\pi (d(t)+\triangle s)}{\lambda}}\right)} \tag{21}$$

where $R_1(t)$ and $R_2(t)$ are the signals received at two different antennas. $H_{s1}(t)$ and $H_{s2}(t)$ are the static signal components, with $a_1(t)$ and $a_2(t)$ are the attenuation and initial phase offsets of the two antennas' dynamic path components, respectively. Compared with the signal propagation length $d(t)$, the difference of target-reflection path length Δs between two antennas is much smaller, which can be considered as a constant within a short period of time.

After the removal of the time-varying base-band chirp signal and the frequency offset, the ratio of LoRa readings of two antennas is now very similar to the CSI-ratio in WiFi set-up. With Möbius transformation, the LoRa signal can thus be used for better sensing, which not only increases the sensing range significantly but also enables through-wall sensing capability.

4 Conclusion

WiFi CSI-based device-free sensing is an important sensing paradigm in today's pervasive environments. While pattern-based approaches fail to reveal the sensing mechanism behind the wireless signals, the model-based approaches have clear advantage of interpretability in understanding the physical properties of wireless signals and characterizing the relationship between CSI and the target's physical parameters. With fundamental physical models, it is possible to understand the relationship between CSI and a target's sensing parameters in a quantitative and interpretable way, so that the human sensing systems can be designed reliably.

As there is a lack of general-purpose sensing model in WiFi-based device-free sensing field, we introduce the Fresnel zone model to the device-free sensing community, and derive a set of properties to guide the wireless system design. In order to further increase the signal-to-noise ratio for sensing and construct orthogonal I/Q signals, we propose the CSI-ratio model leveraging the MIMO technology, to enlarge the sensing range and eliminate the sensing dead zones caused by unusable phase information. Although these two models significantly help to understand the CSI-based device-free sensing mechanism and enable a great number of sensing applications, there are still many research challenges to be addressed in the wireless sensing domain. For example, the two sensing models are good at supporting single person's activity recognition, such as respiration monitoring and finger motion tracking, but are difficult in modeling complex human motions involving multiple human body parts. Therefore, further research efforts are expected to develop new and comprehensive sensing models.

With more and more sensing models proposed, we would have better understanding of the sensing mechanism and properties of various wireless signals, as well as the relationship between received signal and sensing targets' physical parameters. For those complex applications that can not be characterized fully by sensing models, we could combine the pattern-based approaches with the model-based approaches, to ensure the performance and reliability of these applications. It is expected that combining the strengths of model-based approaches and pattern-based approaches would make research breakthroughs in enabling a wide spectrum of applications in everyone's home.

Acknowledgements This research is supported by National Natural Science Foundation of China A3 Project (No. 62061146001), EU CHIST-ERA RadioSense Project, EU Horizon 2020 research and innovation programme IDEA-FAST (No. 853981), National Natural Science Foundation of China (No. 61802373), Youth Innovation Promotion Association, Chinese Academy of Sciences (No. 2020109), and PKU-Baidu Funded Project 2019BD005.

References

Abdelnasser, H., Harras, K.A, Youssef. M.: Ubibreathe: a ubiquitous non-invasive WiFi-based breathing estimator. In: Proceedings of the 16th ACM International Symposium on Mobile Ad Hoc Networking and Computing, pp. 277–286 (2015)

Abdel-Nasser, H., Samir, R., Sabek, I., Youssef, M.: Monophy: mono-stream-based device-free wlan localization via physical layer information. In: 2013 IEEE Wireless Communications and Networking Conference (WCNC), IEEE, pp. 4546–4551 (2013)

Abdelnasser, H., Youssef, M., Harras, K.A.: WiGest: a ubiquitous WiFi-based gesture recognition system. In: 2015 IEEE Conference on Computer Communications (INFOCOM), IEEE, pp. 1472–1480 (2015)

Bahl, P., Padmanabhan, V.N.: Radar: an in-building RF-based user location and tracking system. In: 2000 IEEE Conference on

Computer Communications (INFOCOM), IEEE, vol. 2, pp. 775–784 (2000)
Chen, W., Niu, K., Zhao, D., Zheng, R., Wu, D., Wang, W., Wang, L., Zhang, D.: Robust dynamic hand gesture interaction using LTE terminals. In: 2020 19th ACM/IEEE International Conference on Information Processing in Sensor Networks (IPSN), IEEE, pp. 109–120 (2020)
Chen, Z., Zhang, L., Jiang, C., Cao, Z., Cui, W.: WiFi CSI based passive human activity recognition using attention based blstm. IEEE Trans. Mob. Comput. **18**(11), 2714–2724 (2018)
Chen, L., Xiong, J., Chen, X., Lee, S.I., Zhang, D., Yan, T., Fang, D.: LungTrack: towards contactless and zero dead-zone respiration monitoring with commodity RFIDs. Proc. ACM Interact Mobile Wearable Ubiquitous Technol. **3**(3), 1–22 (2019)
Ding, J., Chandra, R.: Towards low cost soil sensing using Wi-Fi. In: The 25th Annual International Conference on Mobile Computing and Networking, pp. 1–16 (2019)
Gjengset, J., Xiong, J., McPhillips, G., Jamieson, K.: Phaser: enabling phased array signal processing on commodity WiFi access points. In: Proceedings of the 20th Annual International Conference on Mobile Computing and Networking, pp. 153–164 (2014)
Hristov, H.D.: Fresnal Zones in Wireless Links, Zone Plate Lenses and Antennas. Artech House Inc. (2000)
Kotaru, M., Joshi, K., Bharadia, D., Katti, S.: SpotFi: decimeter level localization using WiFi. In: Proceedings of the 2015 ACM Conference on Special Interest Group on Data Communication, pp. 269–282 (2015)
Li, S., Li, X., Niu, K., Wang, H., Zhang, Y., Zhang, D.: AR-Alarm: an adaptive and robust intrusion detection system leveraging CSI from commodity Wi-Fi. In: International Conference on Smart Homes and Health Telematics, pp. 211–223. Springer (2017)
Li, X., Li, S., Zhang, D., Xiong, J., Wang, Y., Mei, H.: Dynamic-MUSIC: accurate device-free indoor localization. In: Proceedings of the 2016 ACM International Joint Conference on Pervasive and Ubiquitous Computing, pp. 196–207 (2016)
Li, C., Liu, M., Cao, Z.: Wihf: enable user identified gesture recognition with WiFi. In: 2020 IEEE Conference on Computer Communications, IEEE, pp. 586–595 (2020)
Li, X., Zhang, D., Lv, Q., Xiong, J., Li, S., Zhang, Y., Mei, H.: IndoTrack: device-free indoor human tracking with commodity Wi-Fi. Proc. ACM Interact. Mobile Wearable Ubiquitous Technol. **1**(3), 1–22 (2017)
Li, S., Liu, Z., Zhang, Y., Lv, Q., Niu, X., Wang, L., Zhang, D.: WiBorder: precise Wi-Fi based boundary sensing via through-wall discrimination. Proc. ACM Interact Mobile Wearable Ubiquitous Technol. **4**(3), 89:1–89:30 (2020)
Liu, X., Cao, J., Tang, S., Wen, J.: Wi-sleep: contactless sleep monitoring via WiFi signals. In: Real-Time Systems Symposium (RTSS), pp. 346–355. IEEE (2014)
Ma, Y., Zhou, G., Wang, S.: WiFi sensing with channel state information: a survey. ACM Comput. Surv. (CSUR) **52**(3), 1–36 (2019)
Palipana, S., Rojas, D., Agrawal, P., Pesch, D.: FallDeFi: ubiquitous fall detection using commodity Wi-Fi devices. Proc. ACM Interact. Mobile Wearable Ubiquitous Technol. **1**(4), 1–25 (2018)
Qian, K., Wu, C., Zhang, Y., Zhang, G., Yang, Z., Liu, Y.: Widar2. 0: passive human tracking with a single Wi-Fi link. In: Proceedings of the 16th Annual International Conference on Mobile Systems, Applications, and Services, pp. 350–361 (2018)
Qian, K., Wu, C., Zhou, Z., Zheng, Y., Yang, Z., Liu, Y.: Inferring motion direction using commodity Wi-Fi for interactive exergames. In: Proceedings of the 2017 CHI Conference on Human Factors in Computing Systems, pp. 1961–1972 (2017)
Sánchez, A.V.D.: Frontiers of research in BSS/ICA. Neurocomputing **49**(1–4), 7–23 (2002)
Schwerdtfeger, H.: Geometry of Complex Numbers: Circle Geometry, Möbius Transformation, Non-Euclidean Geometry. Courier Corporation (1979)
Tan, S., Yang, J.: WiFinger: leveraging commodity WiFi for fine-grained finger gesture recognition. In: Proceedings of the 17th ACM International Symposium on Mobile Ad Hoc Networking and Computing, pp. 201–210 (2016)
Tan, S., Zhang, L., Wang, Z., Yang, J.: MultiTrack: multi-user tracking and activity recognition using commodity WiFi. In: Proceedings of the 2019 CHI Conference on Human Factors in Computing Systems, pp. 1–12 (2019)
Vasisht, D., Kumar, S., Katabi, D.: Decimeter-level localization with a single WiFi access point. In: 13th USENIX Symposium on Networked Systems Design and Implementation (NSDI 16), pp. 165–178 (2016)
Virmani, A., Shahzad, M.: Position and orientation agnostic gesture recognition using WiFi. In: Proceedings of the 15th Annual International Conference on Mobile Systems, Applications, and Services, pp. 252–264 (2017)
Wang, J., Jiang, H., Xiong, J., Jamieson, K., Chen, X., Fang, D., Xie, B.: Lifs: low human-effort, device-free localization with fine-grained subcarrier information. In: Proceedings of the 22nd Annual International Conference on Mobile Computing and Networking, pp. 243–256 (2016)
Wang, Y., Liu, J., Chen, Y., Gruteser, M., Yang, J., Liu, H.: E-eyes: device-free location-oriented activity identification using fine-grained WiFi signatures. In: Proceedings of the 20th Annual International Conference on Mobile Computing and Networking, pp. 617–628 (2014)
Wang, W., Liu, A.X., Shahzad, M., Ling, K., Lu, S.: Understanding and modeling of WiFi signal based human activity recognition. In: Proceedings of the 21st Annual International Conference on Mobile Computing and Networking, pp. 65–76 (2015)
Wang, W., Liu, A.X., Shahzad, M.: Gait recognition using WiFi signals. In: Proceedings of the 2016 ACM International Joint Conference on Pervasive and Ubiquitous Computing, pp. 363–373 (2016)
Wang, H., Zhang, D., Ma, J., Wang, Y., Wang, Y., Wu, D., Gu, T., Xie, B.: Human respiration detection with commodity WiFi devices: do user location and body orientation matter? In: Proceedings of the 2016 ACM International Joint Conference on Pervasive and Ubiquitous Computing, pp. 25–36 (2016)
Wang, H., Zhang, D., Niu, K., Lv, Q., Liu, Y., Wu, D., Gao, R., Xie, B.: MFDL: a multicarrier fresnel penetration model based device-free localization system leveraging commodity Wi-Fi cards (2017). arXiv:1707.07514
Wang, H., Zhang, D., Wang, Y., Ma, J., Wang, Y., Li, S.: RT-Fall: a real-time and contactless fall detection system with commodity WiFi devices. IEEE Trans. Mob. Comput. **16**(2), 511–526 (2016)
Woyach, K., Puccinelli, D., Haenggi, M.: Sensorless sensing in wireless networks: implementation and measurements. In: 2006 4th International Symposium on Modeling and Optimization in Mobile, Ad Hoc and Wireless Networks. IEEE (2006)
Wu, D., Gao, R., Zeng, Y., Liu, J., Wang, L., Gu, T., Zhang, D.: FingerDraw: sub-wavelength level finger motion tracking with WiFi signals. In: Proceedings of the ACM on Interactive, Mobile, Wearable and Ubiquitous Technologies, vol. 4, no 1 (2020)
Wu, D., Zhang, D., Xu, C., Wang, Y., Wang, H.: Widir: walking direction estimation using wireless signals. In: Proceedings of the 2016 ACM International Joint Conference on Pervasive and Ubiquitous Computing, pp. 351–362 (2016)
Wu, C., Yang, Z., Zhou, Z., Liu, X., Liu, Y., Cao, J.: Non-invasive detection of moving and stationary human with WiFi. IEEE J. Sel. Areas Commun. **33**(11), 2329–2342 (2015)

Wu, D., Zhang, D., Xu, C., Wang, H., Li, X.: Device-free WiFi human sensing: from pattern-based to model-based approaches. IEEE Commun. Mag. **55**(10), 91–97 (2017)
Xiao, J., Wu, K., Yi, Y., Wang, L., Ni, LM.: Pilot: passive device-free indoor localization using channel state information. In: 2013 IEEE 33rd International Conference on Distributed Computing Systems, IEEE, pp. 236–245 (2013)
Xie, Y., Li, Z., Li, M.: Precise power delay profiling with commodity Wi-Fi. In: Proceedings of the 21st Annual International Conference on Mobile Computing and Networking. ACM (2015)
Xie, Y., Xiong, J., Li, M., Jamieson, K.: md-Track: leveraging multi-dimensionality for passive indoor Wi-Fi tracking. In: The 25th Annual International Conference on Mobile Computing and Networking, pp. 1–16 (2019)
Xin, T., Guo, B., Wang, Z., Wang, P., Lam, J.C.K., Li, V., Yu, Z.: FreeSense: a robust approach for indoor human detection using Wi-Fi signals. Proc. ACM Interact. Mobile Wearable Ubiquitous Technol. **2**(3), 1–23 (2018)
Yang, Y., Cao, J., Liu, X., Xing, K.: Multi-person sleeping respiration monitoring with COTS WiFi devices. In: 2018 IEEE 15th International Conference on Mobile Ad Hoc and Sensor Systems (MASS), IEEE, pp. 37–45 (2018)
Youssef, M., Mah, M., Agrawala, A.: Challenges: device-free passive localization for wireless environments. In: Proceedings of the 13th Annual ACM International Conference on Mobile Computing and Networking, pp. 222–229 (2007)
Zeng, Y., Pathak, P.H., Mohapatra, P.: WiWho: WiFi-based person identification in smart spaces. In: 2016 15th ACM/IEEE International Conference on Information Processing in Sensor Networks (IPSN), IEEE, pp. 1–12 (2016)
Zeng, Y., Wu, D., Xiong, J., Zhang, D.: Boosting WiFi sensing performance via CSI ratio. IEEE Pervasive Comput. (2020)
Zeng, Y., Wu, D., Gao, R., Gu, T., Zhang, D.: FullBreathe: full human respiration detection exploiting complementarity of CSI phase and amplitude of WiFi signals. Proc. ACM Interact Mobile Wearable Ubiquitous Technol. **2**(3), 1–19 (2018)
Zeng, Y., Wu, D., Xiong, J., Yi, E., Gao, R., Zhang, D.: FarSense: pushing the range limit of WiFi-based respiration sensing with CSI ratio of two antennas. Proc. ACM Interact. Mobile Wearable Ubiquitous Technol. **3**(3), 1–26 (2019)
Zeng, Y., Wu, D., Xiong, J., Liu, J., Liu, Z., Zhang, D.: MultiSense: enabling multi-person respiration sensing with commodity WiFi. Proc. ACM Interact Mobile Wearable Ubiquitous Technol. **4**(3), 1–29 (2020)
Zhang, D., Wang, J., Jang, J., Zhang, J., Kumar, S.: On the feasibility of Wi-Fi based material sensing. In: The 25th Annual International Conference on Mobile Computing and Networking, pp. 1–16 (2019)
Zhang, J., Wei, B., Hu, W., Kanhere, S.S.: WiFi-id: Human identification using WiFi signal. In: 2016 International Conference on Distributed Computing in Sensor Systems (DCOSS), IEEE, pp. 75–82 (2016)
Zhang, D., Zhang, F., Wu, D., Xiong, J., Niu, K.: Fresnel zone based theories for contactless sensing. In: Contactless Human Activity Analysis, p. 145 (2021)
Zhang, D., Wang, H., Wu, D.: Toward centimeter-scale human activity sensing with Wi-Fi signals. Computer **50**(1), 48–57 (2017)
Zhang, F., Zhang, D., Xiong, J., Wang, H., Niu, K., Jin, B., Wang, Y.: From Fresnel diffraction model to fine-grained human respiration sensing with commodity Wi-Fi devices. Proc. ACM Interact Mobile Wearable Ubiquitous Technol. **2**(1), 1–23 (2018)
Zhang, F., Wu, C., Wang, B., Lai, H.Q., Han, Y., Liu, K.R.: Widetect: robust motion detection with a statistical electromagnetic model. Proc. ACM Interact. Mobile Wearable Ubiquitous Technol. **3**(3), 1–24 (2019)
Zhang, F., Niu, K., Xiong, J., Jin, B., Gu, T., Jiang, Y., Zhang, D.: Towards a diffraction-based sensing approach on human activity recognition. Proc. ACM Interact Mobile Wearable Ubiquitous Technol. **3**(1), 1–25 (2019)
Zhang, F., Chang, Z., Niu, K., Xiong, J., Jin, B., Lv, Q., Zhang, D.: Exploring LoRa for long-range through-wall sensing. Proc. ACM Interact Mobile Wearable Ubiquitous Technol. **4**(2), 1–27 (2020)
Zheng, Y., Zhang, Y., Qian, K., Zhang, G., Liu, Y., Wu, C., Yang, Z.: Zero-effort cross-domain gesture recognition with Wi-Fi. In: Proceedings of the 17th Annual International Conference on Mobile Systems, Applications, and Services, pp. 313–325 (2019)
Zou, H., Zhou, Y., Yang, J., Gu, W., Xie, L., Spanos, C.J.: WiFi-based human identification via convex tensor shapelet learning. In: Thirty-Second AAAI Conference on Artificial Intelligence (2018)

Dan Wu received a Ph.D degree in Computer Science from Peking University in 2020. He is currently an associate research fellow with the department of Computer Science and Technology at Peking University, China. His research interests include wireless sensing and mobile computing.

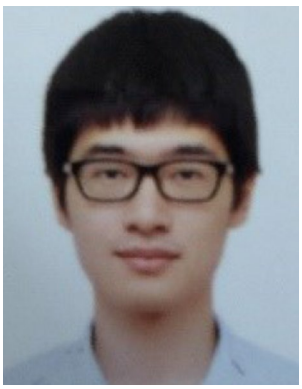

Youwei Zeng received a B.E degree in Software Engineering from Zhejiang University in 2016. He is currently working toward the Ph.D degree in Computer Science in the department of Computer Science and Technology, Peking University. His research interests include ubiquitous computing and mobile computing.

Fusang Zhang received his M.S. and Ph.D. degrees in computer science from the Institute of Software, Chinese Academy of Sciences, Beijing, China, in 2013 and 2017, respectively. He is currently an Associate Professor with the Institute of Software, Chinese Academy of Sciences. His current research interests include mobile and pervasive computing, ad hoc network, and wireless contactless sensing.

Daqing Zhang is a chair professor with the Key Laboratory of High Confidence Software Technologies, Peking University. He obtained his Ph.D. from the University of Rome "La Sapienza," Italy in 1996. His research interests include context-aware computing, urban computing, mobile computing, big data analytics, and more. Dr. Zhang is the IEEE fellow and the fellow of the European Academy of Sciences. he is also the Associate Editor for four journals including ACM Transactions on Intelligent Systems and Technology. He has been a frequent Invited Speaker in various international events on ubiquitous computing. He is the winner of the Ten Years CoMoRea Impact Paper Award at IEEE PerCom 2013, the Best Paper Award at IEEE UIC 2015/2012 and the Best Paper Runner Up Award at Mobiquitous 2011. He is a member of the China Thousand-Talent Program.